The International Journal of Advanced Manufacturing Technology (2023) 124:1253–1271
https://doi.org/10.1007/s00170-022-10577-6

ORIGINAL ARTICLE

Spindle bearing fault detection in high-speed milling machines in non-stationary conditions

Mourad Lamraoui[1]

Received: 1 July 2022 / Accepted: 22 November 2022 / Published online: 30 November 2022

Abstract
Vibration monitoring of CNC high-speed machining (HSM) centers under non-stationary conditions, characterized by varying operating parameters and uncertainties affected by the change of speed and load during operation currently presents a particular challenge. Therefore, bearing condition monitoring is important. Indeed, this variation has a considerable impact on the vibratory response delivered by the accelerometers and therefore can mask any fault. The change in speed causes considerable changes in the spectrum of the vibration such that defect signatures become almost undetectable with conventional tools. The order tracking method based on time–frequency representation is regarded as an effective tool for fault detection of bearings with varying rotating speeds. This study aims to propose non-stationary tools based on tachometer order tracking to detect bearing faults in high-speed milling centers during run-up and coast-down conditions. Developed tools are compared to stationary technics in this study, remaining limited to detect faults. Indeed, the speed variation would cause spectrum smearing if classic tools are used in non-stationary conditions. These latter methods are based on constant rotating speed and would fail to detect faults of bearings with variable spindle rotating speeds.

Keywords HSM · CNC · Order tracking · Non-stationary condition · Bearings · RPM-Order · Time–frequency · Monitoring

1 Introduction

High-speed milling machines (HSM), which are frequently employed in machining operations, are essential in industrial manufacturing. They produce high-quality products with tighter tolerances because of their low cutting forces and high material removal rates. Unfortunately, process instability has a negative impact on product surface polish, lowers dimensional accuracy, speeds up tool wear, and can even result in spindle-tool unit failure. In the industrial world, machine monitoring is becoming more and more crucial as a result of the requirement to increase machine dependability and minimize production capacity loss owing to failures brought on by various flaws.

In the field of rotating equipment monitoring, the use of vibration signals is relatively contemporary. It takes a high level of expertise in the currently existing approaches to successfully apply them; new techniques are needed to enable unqualified operators to make trustworthy decisions without understanding the mechanism of the system. One of the main research challenges in the field of rotating machinery diagnostics is machine's condition monitoring in non-stationary operation. Applications are everywhere: in vehicles, energy systems, and manufacturing facilities. For these reasons, the current work is focused on measurement techniques and signal processing methods for tracking the condition of bearings exposed to non-stationary operating conditions in high-speed machining centers.

Monitoring the condition of machines while they are in non-stationary operation is one of the main research issues in the field of rotating machine diagnostics, such as gearboxes [1, 2]. The majority of published works center on validating condition monitoring methodologies through test bench measurement surveys. For instance, in [3], the viability of instantaneous angular velocity (IAS) monitoring as a way to keep track of the gear's health subjected to varying load conditions was investigated. A conventional shaft encoder can be used to monitor the instantaneous angular velocity of a gear shaft to detect changes in the condition of the gear, according to an experimental study on a test rig. [4] Provides a reference study on the topic.

✉ Mourad Lamraoui
mourad.lamraoui@univ-st-etienne.fr

[1] University of Lyon, Jean Monnet Saint Etienne University, IUT de Roanne, LASPI, Roanne, France

On a gearbox test rig, tests were performed with varying degrees of tooth damage severity and the capacity to apply varying loads to the gear system. Various intensities of sinusoidal, step-and-jerk, and fluctuating constant loads were weighed. To account for the variation in rotational speed brought on by the fluctuating loads, the test data was sequentially tracked and averaged synchronously with the shaft rotation.

Cyclostationarity has gained popularity in recent years across a variety of applications, such as acoustic analysis and mechanical vibrations. The general idea is to include signals whose statistical properties change periodically over time in the class of stationary signals. The similarities in [5], Differences between cyclic and classical spectral analysis are discussed, as well as potential pitfalls. The preservation of the cycle energy variations can help to estimate the influence of the rotation speed variation on the signal energy, according to a method proposed in [6] for extracting the second-order cyclostationary components of a vibrational signal. A wind turbine, which is a significant validation case, is provided. An energy conversion device operating under harsh non-stationary circumstances is a classic example.

The fact that monitoring the actual state of machines operating in their working environment is much more challenging than doing so in a lab underscores a crucial point about condition monitoring of machines operating under non-stationary conditions. Power conversion systems, like wind turbines, are a classic example because they are subject to random loads and wind turbulence. Monitoring the rolling elements and bearings is particularly challenging for MW-scale wind turbines because they typically use a gearbox to convert slow rotor rotation into fast generator rotation [7–9]. It should also be noted that the control system moves a very high inertia nacelle in response to changes in wind speed, which may have an impact on things like yaw [10, 11] and/or pitch [12] life. The critical point for small horizontal axis wind turbines is that they are significantly affected by fatigue because of the load variability that is modulated by extremely high rotational speeds of the small rotor [13].

Machine tools are widely used in a variety of industries, including the automotive, aerospace, and military. These industries are currently working to improve their productivity, precision, and tolerances in order to create higher-quality products with less waste and impact on the environment. Machine tools are composed of several subassemblies where the spindle unit is an important structural element located in different positions, depending on the machine tool configuration. The spindle unit plays an important role in the functionality and performance of a machine tool. The spindle performs two important functions: first, to give precise rotational motion to the tool (e.g., drilling, milling, and grinding) or to the workpiece (e.g., turning). Second, it transmits energy to the cutting area to remove material. Spindle problems are one of the most important sources of machine tool downtime in the manufacturing industry.

In a German study [14], where maintenance information was collected from 250 machine tools in the automotive manufacturing sector, four major subsystems were identified as being responsible for most downtimes. Within these, the spindle and tool changer accounted for 26% of the downtime within these four subsystems, being the second major cause after the drive axes. The degree of vibration in spindle units is regarded as a crucial factor in determining the health of a machine over its lifetime in machine tools. This parameter is frequently linked to a broken bearing, an imbalance, or a spindle issue. Although vibration levels are significant, there is no ISO standard for determining spindle health. The planning of maintenance chores for these high-precision systems is somewhat hampered by this circumstance. Several authors propose that bearing damage is the primary cause of spindle failure. In the industrial sector, spindle bearings are considered "the most sensitive components" [14].

In fact, bearing damage is by far the most common in motor spindles according to [15]. Another study, within the aerospace industry, cited in [16] indicates that bearing damage accounts for 60% of electrospindle failures. Due to the importance of bearing damage on spindle life and therefore condition monitoring, this will be discussed in more detail in this article in stationary and non-stationary conditions. An example of anomalous operating conditions in spindles that lead to bearing damage is tool breakage. As pointed out by [17] in their real-time monitoring of three motor spindles over a 7-month period in the aerospace industry, tool breakage was attributed as the primary cause in the front bearing of one of the spindles. The authors explain that during tool failure (0.5 s), high forces were generated, which caused the ceramic balls to indent on the steel raceway. This indentation leads to plastic deformation. This damage is further developed by strong vibrations due to cutting with a broken tool (for several minutes before being discovered) and harmonics produced by the passage of the tool frequency.

Bearings are critical components of rotating equipment and machine tool spindles are no exception. As mentioned earlier, many researchers and experienced professionals attribute bearing damage as the leading cause of spindle failure. Fortunately, bearing failure has been the subject of much research over the past few decades, so there is a great deal of literature research on the subject. Although little research has been conducted on the detection of bearing damage on machine tool spindles, the purpose of this subsection is to provide an overview of different approaches to detect and evaluate bearing damage on spindles. The focus will be on the methods, results, and limitations of these studies. In order to identify localized bearing deterioration on bearings, Hoshi proposed using the vibration spectrum as an indicator [18]. A different study [19] compares several

spindles-bearing monitoring methods. These included temperature, vibration, and sound emissions. In this instance, just like in Hoshi's work, the spindle bearing was overloaded in an effort to cause damage. However, axial, radial, dynamic static, and spindle-driven stresses were utilized in this experiment along with a motorized spindle. Improved indications for evaluating support circumstances have also been suggested by other researchers, such as [17]. The authors of this study investigated bearing failures brought on by actual operating conditions in an industrial setting. The vibration evolution of three identical electro spindles utilized in the aerospace industry was investigated by the authors.

The experimental development of an instrumented smart spindle, which can assess tool wear by monitoring axial shaft displacement in real-time and therefore applicable to drilling processes, is shown by the authors in [18]. Cutting trials utilizing a Kistler dynamometer and an instrumented smart spindle have revealed a strong correlation between measurements of the axial displacement and axial drilling force. The drilling engagement with each copper layer can be determined using the axial displacement. The instrumented smart spindle can also be used to prevent overloading a thrust bearing and, most critically, to identify tool wear as it occurs. A method for evaluating the health of motorized spindles was proposed by Yang H. and other authors in [19] using an optimized variational mode decomposition (VMD) and a Gaussian mixture model-hidden Markov model (GMM-HMM). The motorized spindle performance monitoring test platform is used to conduct the rotor unbalanced fault experiment. The tested motorized spindle's condition is assessed using the suggested method, and the results demonstrate its superiority.

In the current industry 4.0 Era, intelligent spindles are core components of the next generation of intelligent/smart machine tools. Clarifying the concept of intelligent spindles and offering an in-depth review of the state-of-the-art in related technologies are the targets of the paper's work in [20]. The authors then describe the required qualifications, key enabling technologies, and anticipated intelligent functions before proposing a new integrated concept for intelligent spindles.

The operating regime (i.e., speed and/or load) is assumed to be constant or maybe varying in a stationary manner by all of these strategies. Unfortunately, in order to complete the duties for which they were intended, the majority of the machines monitored in the industry operates in non-stationary regimes. These methods fall short in this instance of vibration signal analysis. The scientific world has been preoccupied with this issue for the past 10 years, and sophisticated signal-processing techniques have been developed to handle regime fluctuations. The theoretical formalization of the non-stationary framework is provided in [21] by the authors through the methodical creation of novel signal processing tools. Assumed to be known a priori, the non-stationarity of the regime in this work is only that of the velocity, which is defined as changing velocity and constant load. The strategy is to expand cyclostationary framework with its specialized tools to reach this goal. By distinguishing between two different signature kinds, authors have devised a technique. The first class consists of first-order cyclostationary deterministic signals. The suggested remedy entails extending the first-order cyclostationary class to encompass deterministic signals with variable speeds. This is known as first-order cyclo-non-stationary. The second category consists of second-order cyclostationary random signals, which are periodically correlated random signals. Three different but complimentary points of view have been put out to address the variances brought on by the operating speed's non-stationarity. A cyclostationary angle approach is used in the first, an envelope-based technique in the second, and a cyclo-non-stationary (second order) approach in the third. Numerous instruments have been created, and real-world and computer-simulated vibration signals have been used to examine how well they operate. Only a few strategies have been examined under load/speed variation, and condition monitoring is typically used to diagnose the performance of mechanical systems under steady state settings, such as typically at a constant speed.

Cutting parameters, the cutting state, and traditional time–frequency domain cutting features all change significantly under variable cutting conditions. Recurrence plot (RP) is a time series method that can reflect the non-stationary characteristics and state differences of the signal system to analyze the cutting force signal in the cutting process. It was proposed by authors in [22] in order to achieve precise monitoring of chatter under such cutting conditions. According to experimental results, the method can accurately determine the stable cutting state and chatter state all through variable cutting conditions.

For the identification of bearing problems in non-stationary settings and with gear noise interference, the authors of [23] suggest a comprehensive demodulation transformation. In [24], the authors looked into the viability of employing time–frequency analysis methods like the Wigner-Ville distribution and its benefits in the diagnosis of machines operating in variable regimes by spotting parasitic energy leakage in various spectral regions. A comparable piece of work for the monitoring of variable speed gearboxes may be found in [25]. To address the impact of speed fluctuation on the vibration of gear transmissions, [26] proposes two indicators normalized by the instantaneous frequency. Authors in [27] describe the use of the instantaneous angular spectrum to track torsional vibrations in a diesel engine. It was discovered that the order analysis can only manage the frequency responses due to changes in speed; it cannot, however, handle changes in

resonant energy or the complexity of modulation effects that follow. Complexity brought on by the signal's modulation effects. In order to try to divide the velocity profile into various pseudo-stationary regimes, a new method to generalize the synchronous averaging technique has been devised in [28]. To identify fault characteristics for variable speed machines, the same researchers used a different technique of spectral preprocessing mixed with envelope analysis in [29]. A variety of methods have been created to detect bearing faults over time and at various speeds. Order tracking [26–29] is one of these techniques that is thought to be effective.

The order tracking analysis is a measurement method appropriate for non-stationary and variable speed machines. It calls for sampling the vibration signal at fixed angle intervals, and as a result, at a sampling rate proportional to the machine's shaft speed. The frequency spectrum components can thus be represented in a waterfall plot as stationary lines against orders (multiples of the shaft rotation) rather than frequency, in Hz. An order spectrum relates the signal's amplitude and phase to the harmonic order of the rotational frequency. This means that regardless of the machine's speed, a harmonic or subharmonic order component remains in the same analysis line.

Indeed, in the order tracking method, the original signal is resampled at constant angle intervals and, thus, the fault-induced pulses are reordered to be equal in the angular domain. A stationary signal in the angular domain is created by translating the non-stationary signal in the time domain. The velocity smearing and spectrum smearing effects are eliminated by the order tracking method. The diagnosis of ball bearings in high-speed milling centers under stationary and non-stationary settings is the main topic of this research. Non-stationary operating conditions have an impact on the vibration signal, disguising the presence of impending flaws or masking the impact of a defect caused by a machine's higher energy impacts, that is, impacts from the machine's regular operation. In this study, a tachometer order analysis approach for high-speed milling center bearing failure diagnosis under variable rotational speed conditions is provided.

The rest of the document is structured as follows. The order tracking algorithm is introduced in Section 2 (OTA). The experimental equipment used to carry out this study is described in Section 3 of the article. The stationary analysis is introduced in Section 4. This section studies and analyzes indicators of frequency, time–frequency, and stationary statistics. The method proposed in Section 5 is used to identify bearing faults. On vibration signals, a variety of non-stationary methods 5 based on order tracking, including RPM order, average order spectrum, and relative RMS, are examined and put to the test. Finally, Section 6 draws conclusions.

2 Order tracking algorithm "OTA"

The study of rotation-induced vibrations in rotating systems is known as order analysis. These vibrations' frequencies are frequently inversely correlated with rotational speed. The orders are the constants of proportionality. Under most experimental circumstances, the rotational speed is typically determined separately and varies over time. Resampling and interpolation of the observed signal are required for proper analysis of rotation-induced vibrations in order to acquire a fixed number of samples per cycle. This method converts signal elements into constant tones whose frequencies are multiples of the rotational speed that are constant. This transformation lessens spectral component interference, which develops when the frequency fluctuates quickly over time [30]. The rpm-order representation is performed by following these steps:

1. In the first step, the rotational speed signal RPM is extracted from the tachometer pulse signal. The tachometer signal's low and high states are first determined. Then, the beginning and ending times of each pulse are calculated. The time of each pulse is then determined by averaging these readings. After that, the time intervals between the pulse centers and the RPM values are computed at the midpoints of the interval using $\mathrm{RPM} = 60/\Delta t$. Finally, linear interpolation is used to estimate the rotational speed signal.
2. The second step is to calculate the phase angle using the equation for the time integral of the rotational speed (1). In this instance, the RPM signal is estimated using the tachometer signal:

$$\varnothing(t) = \int_0^t \frac{\mathrm{RPM}(\tau)}{60} d\tau. \tag{1}$$

3. Signal upsampling and lowpass filtering: this process prevents high-frequency components from being aliased when the signal is interpolated at unsampled time points.
4. In the phase domain, linearly interpolate the sampled signal upwards on a regular grid. Due to the variable speed operations that spread the spectrum, the initial signal is not stationary in the time domain. Based on the estimated instantaneous phase information from the first step, the original signal is resampled at equal angular intervals to get around this issue. Based on the estimated instantaneous frequency from the signal, the formula calculates the instantaneous phase. As a result, the time-domain non-stationary signal is transformed into an angular-domain stationary signal.

5. The sample rate and the system's maximum rotational speed together determine the measurement's highest accessible order:

$$O_{\max} = \frac{Fs/2}{\max\left(\frac{\text{RPM}}{60}\right)} \tag{2}$$

Fs is the sample frequency.

To capture this highest accurately, it is necessary to sample the signal at twice $O_{\max}$ at least. For better result, the signal is oversampled by an extra factor of 4. The resulting phase-domain sample rate, f_p is:

$$f_p = 4 \times 2 \times O_{\max} \tag{3}$$

The default order resolution, r, is:

$$r = \frac{f_p}{256} = \frac{4 \times 60}{256} \frac{2 \times Fs/2}{\max(\text{RPM})} = \frac{15}{16} \frac{Fs}{\max(\text{RPM})} \tag{4}$$

6. The interpolated signal's short-time Fourier transform (STFT) is computed as the final step. By default, the function divides the signal into L-sample segments and windows each of them with a flat-top window. There are N_{overlap}

$$N_{\text{overlap}} = \min\left(\lceil \frac{p_{\text{overlap}}}{100} \times 100 \rceil, L - 1\right) \tag{5}$$

samples of overlap between adjoining segments, where p_{overlap} is equal to 50% in this application. The DFT length is set to L. The resolution is related to the sample rate and segment length through

$$r = \frac{kf_p}{L} \tag{6}$$

where k is the equivalent noise bandwidth of the window without a unit. In fact, the equivalent noise bandwidth of a window is the width of a rectangle whose area contains the same total power as the window. The height of the rectangle is the peak-squared magnitude of the window's Fourier transform. Assuming a sampling interval of 1, the total energy for the window, $w(n)$, can be expressed in the frequency or time-domain as:

$$\int_{-\frac{1}{2}}^{\frac{1}{2}} |W(f)|^2 df = \sum_n |w(n)|^2 \tag{7}$$

The peak magnitude of the window's spectrum occurs at $f = 0$. This is given by $|W(0)|^2 = \left|\sum_n w(n)\right|^2$. The width of the equivalent rectangular bandwidth (k) is obtained by dividing the area by the height and the result is presented in this equation:

$$k = \frac{\int_{-0.5}^{0.5} |W(f)|^2 df}{|W(0)|^2} = \frac{\sum_n |w(n)|^2}{\left|\sum_n w(n)\right|^2} \tag{8}$$

3 Methodology and taxonomy

Like all rotating machines, machining centers contain parts wear, in particular the bearings, which are subject to dynamic stresses inherent in their modes of operation. Cutting forces, centrifugal forces, high rotation speeds as well as the contaminated environment influence the dynamic behavior of the milling machine spindles and the useful lifetime of bearings. However, statistics reveal that only 3% of bearings reach their theoretical lifespan, unlike the remaining 97%, which fail to reach their theoretical lifetimes due to multiple reasons such as lubrication inadequate, contamination of the lubricant, poor assembly, or inadequate operating conditions inducing excessive stresses (vibrations, temperature, speed, current flow, overload, etc.). This observation is reinforced in the CNC by the highly transient nature of the operating conditions—amplitudes, directions, frequencies of cutting forces, and speed of rotation.

From there, it becomes clear that the dynamic behavior of CNCs is strongly linked to the health of the most critical components, such as bearings. Bearing defects can be detrimental to the machine, especially if they are coupled with other machining conditions, producing regenerative chatter phenomena.

In fact, specialists in machining use stability lobe diagrams, making it possible to locate the conditions of stable cuts depending on the operating parameters. This diagram requires knowledge of the dynamic characteristics of the tool-tool holder assembly [31]. These characteristics may vary in the operational mode of the machine and in the presence of bearing defects [32]. A review of the most recent and pertinent studies in the area of dynamics in micro-milling processes is provided in [33] by Heitz, T. and all other authors. The definition of dynamics in machining is revised, along with the mathematical principles used in micro-milling with consideration of the size effect and common phenomena impacting the dynamic model. They also discuss common techniques for detecting vibration and chatter as well as techniques for suppressing it.

With this in mind, this article presents a variety of methods for detecting bearing defects in a machining center in stationary and non-stationary conditions. In stationary conditions, the acquired vibratory signals will be processed in the time, frequency, and time–frequency domains. The evolution of certain statistical indicators is also presented. In non-stationary conditions, up run and

coast run, signals are processed in order domain and the order tracking algorithm is applied to detect and track the bearings defects.

The process is initiated by acquiring data from the system in stationary and non-stationary conditions and in the presence of a bearing defect. For this reason, accelerometers and tachometer sensors are implemented on the system in two positions at different directions to collect multiaxial data. Then, the collected data is processed, analyzed, and interpreted using simple and advanced signal-processing tools. The different steps of the proposed methodology are discussed in detail in the following subsections.

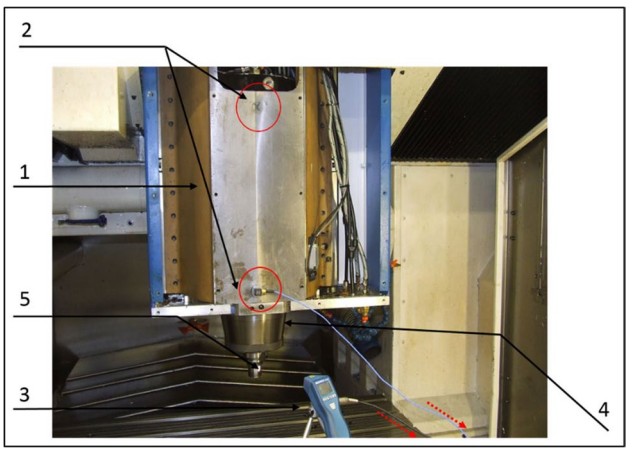

Fig. 1 Experimental setup: (1) non-rotating part of the spindle, (lower and higher level), (2) three-axial accelerometer, (3) tachometer sensor, (4) holder, and (5) reflective tape. Red arrows indicate the data transfer to the data acquisition system

3.1 Experimental data acquisition

All the experimental milling processes are performed in non-stationary conditions (up and down run) and in stationary conditions in different rotation's speeds (from 3000 to 28000 rpm). The accessibility of the rotor and the structural complexity of the electro-spindle make it difficult to insert the sensors. Indeed, only the tool is accessible from the outside. For convenience, the accelerometers are placed on the spindle body at the bearing's levels.

The different tests are carried out without machining and using a vertical machine center K2X10 which is able to operate at high rotational speeds (28000 rpm). Figure 1 shows the experimental setup used to achieve tests at different conditions. Three-axial piezoelectric accelerometers are used to capture the vibrations from 1 to 10 kHz. The measurement range is ± 500 g pk. The accelerometers are attached to the non-rotating part of the spindle (spindle support) on the lower and upper part of the bearing level (Fig. 1). The tachometer sensor is placed in front of the tool holder and makes it possible to deliver a square signal whose frequency is the frequency of rotation of the spindle. Data acquisition was conducted with a 24-bit accuracy in two cases (Fig. 6). It is configured to obtain signals during 1 s with a maximum sampling rate of 48 kHz for each spindle speed and 10 s for up/coast run. The acquisition is controlled by the BETAVIB system. The parameters and procedure of experimental data acquisition are synthesized in Fig. 2.

The most relevant information in the spectrum is the presence of frequency components at frequencies that are usually inaccessible to standard accelerometers. Rotation at 28000 rpm (466.66 Hz) implies bearing fault frequencies between 4000 and 6000 Hz (see Table 4), whereas the

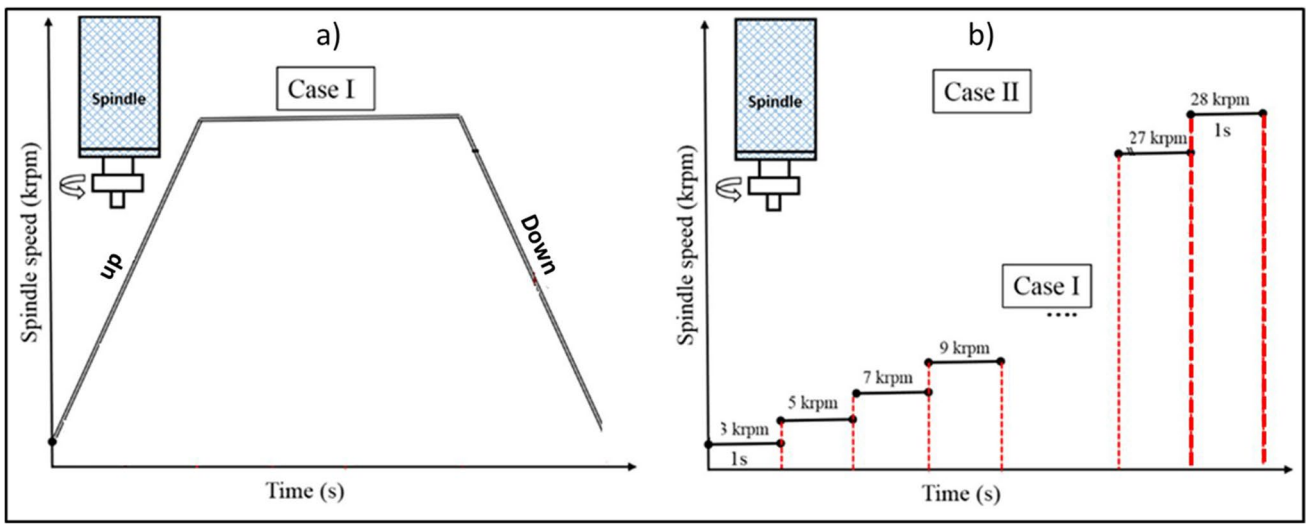

Fig. 2 The proposed approach for testing several spindle speeds in two cases. **a** (Cass I) up/down diagram: in non-stationary conditions, from 3000 to 28000 rpm. **b** (Case II) staircase diagram: in stationary conditions at different spindle speed during 1 s for each speed

bandwidth of industrial (conventional) accelerometers barely reaches this range. The fault frequencies, which generally occur at the 2nd or 3rd harmonic, are not detectable, because the cut-off frequencies are between 5 and 8 kHz depending on the nature of the fastener used (magnet, wax, screwed…). For this experimental analysis (Fig. 4), particular attention was paid to the measurement chain, and PCB accelerometers type 352C04—cutoff frequency starting at 15 kHz—were used to reach the frequencies of interest as well as their 1st, 2nd, and 3rd order harmonics, with a sensitivity of 10 mV/g allowing the measurement of high vibratory amplitudes—especially in cross-section—without saturating the sensor (Table 1).

The electro-spindle is the most sensitive part of a high-speed machine. Indeed, it is subjected to high power, vibrations, and high rotational speeds (today Huron spindles rotate up to 28,000 rpm—1). This is the part the more complex and expensive the machine. To optimally use an HSM machine, it is necessary to master the dynamic behavior of its spindle and detect all faults that may appear, in particular, bearing faults. Therefore, the different parameters machining (depth of cut, cutting and feed speed, etc.) are adapted in order to obtain high productivity and manufacturing quality, while preserving the means of production. Figure 3 shows the schematic diagram of HURON electro-spindle UGV-28000 rpm.

Table 1 Summary of the machining for bearing fault tests

Case	Test no	Spindle speeds (Krpm)
I. Stationary conditions (case II)	1 … 16	3, 5, …28
II. Non-stationary conditions (case I)	Run up and run down	From 3 to 28 Krpm

3.2 Bearing characteristics

Huron electro-spindle (28000 rpm, 70 kW) has been studied and monitored. The bearing arrangement can be found in Fig. 3. It is equipped with hybrid ball bearings at the front and at Table 2 presents the bearing geometric characteristics and the bearing fault orders/frequencies that have been provided by the manufacturer. In this study, theoretically calculated frequencies are compared with experimentally determined frequencies.

Their calculation formulas are given in Table 3.

θ is the contact angle, d is the ball or roller diameter and D is the pitch circle diameter of the bearing. According to the above equations, the bearing fault characteristics in the order domain are independent of the shaft rotating speed. Therefore, bearing fault detection based on the order domain can exclude the influence of speed fluctuation.

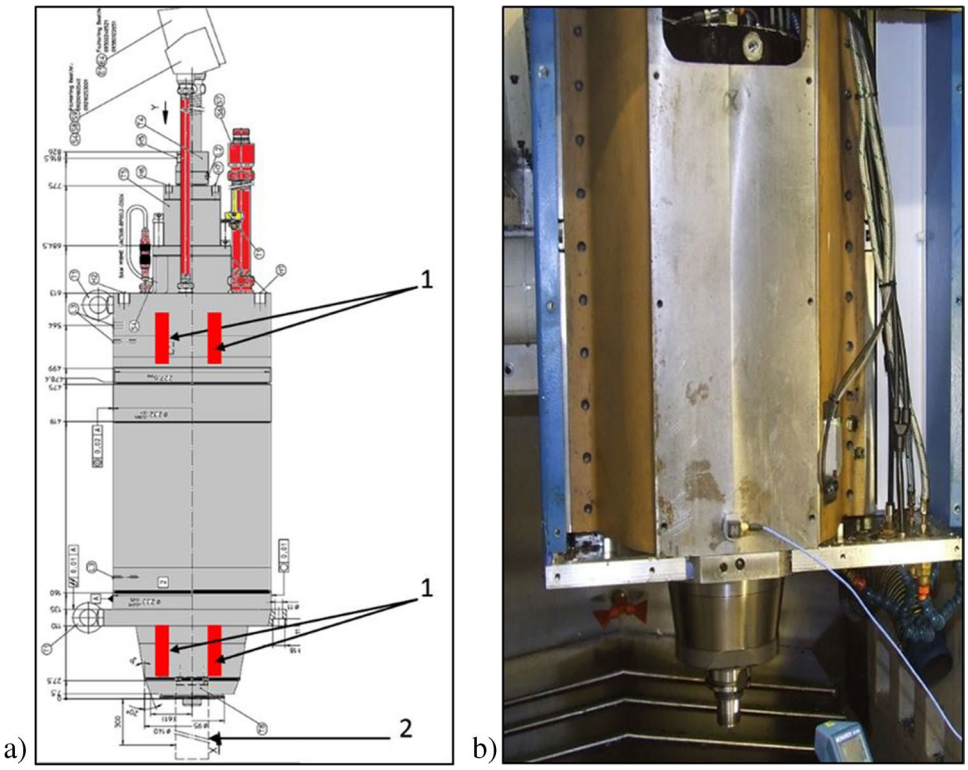

Fig. 3 **a** Schematic diagram of HURON electro-spindle UGV-28000 rpm, (1) hybrid ball bearings, (2) tool. **b** Real HURON electro-spindle UGV

Table 2 Bearings characteristics

		Outer race		Inner race		Cage	
	Number of balls *n*	*BPFO*	*BPOO*	*BPFI*	*BPOI*	*FTF*	*FTO*
Hybrid ball bearings	20	8.84**fr*	8.84	11.1**fr*	11.1	0.44**fr*	0.44

fr, spindle frequency rotation; *O*, order; *BPFO*, ball pass frequency outer; *BPOO*, ball pass order outer; *BPFI*, ball pass frequency inner; *BPOI*, ball pass order inner; *FTF*, fundamental train frequency; *FTO*, fundamental train order; *n*, number of balls; *Nb*, number of balls

Table 3 Calculation formulas

$BPFO =$	$fr.\frac{n}{2}\left\{1-\frac{d}{D}\cos\theta\right\};$	$BPOO =$	$\frac{n}{2}\left\{1-\frac{d}{D}\cos\theta\right\}$
$BPFI =$	$fr.\frac{n}{2}\left\{1+\frac{d}{D}\cos\theta\right\};$	$BPOI =$	$\frac{n}{2}\left\{1+\frac{d}{D}\cos\theta\right\}$
$FTF =$	$fr.\frac{1}{2}\left\{1-(\frac{d}{D}\cos\theta\right\};$	$FTO =$	$\frac{1}{2}\left\{1-(\frac{d}{D})^2 cos^2\theta\right\}$

4 Stationary analysis

4.1 Frequency analysis

To properly identify the signatures of a particular fault during the diagnosis of rotating machines in the frequency domain, it is very important to properly configure the spectrum (spectral resolution, windowing, etc.) and to know the kinematics of the installation to be able to target the specific signatures of this fault. For example, in the case of a bearing, characteristic frequencies such as BPFO, BPFI, and FTF or their harmonics will be determined. The severity of the fault is related to the values of the amplitudes corresponding to these frequencies and their harmonics. The more the amplitude of the peaks at these frequencies is significant and the greater the number of harmonics and modulation frequencies is, the more advanced the defect is in the degradation stage.

The frequency spectrum of vibration signal acquired in stationary conditions is plotted for each rotational speed which varies from 3000 to 28000 rpm and identified the bearing fault frequencies namely BPFO, BPFI, and FTF. Table 4, below summarizes all the experimental values identified from the frequency spectra and the theoretical values obtained by applying the formulas given in Table 3. The theoretical values are close to the experimental values. This difference can be explained by the influence of ball sliding which will introduce fluctuations in the speed of rotation and therefore fluctuations in the characteristic frequencies of the defect.

Table 4 Experimental and theoretical frequency faults (BPFO, BPFI, and FTF) as a function of spindle speed

Spindle speed (Rpm)	Spindle speed (Hz)	Experimental FTF frequencies	Theoretical FTF frequencies	Experimental BPFI frequencies	Theoretical BPFI frequencies	Experimental BPFO frequencies	Theoretical BPFO frequencies
3000	50,00	22,46		583,00	585,90	438,86	440,20
5000	83,33	37,43		971,67	974,90	731,43	733,20
7000	116,67	52,40	52,70	1360,33	1365,00	1024,01	1027,00
9000	150,00	67,37	67,38	1749,00	1754,00	1316,58	1320,00
11000	183,33	82,34	82,03	2137,67	2143,00	1609,15	1614,00
13000	216,67	97,31	96,68	2526,33	2531,00	1901,73	1907,00
15000	250,00	112,28	112,10	2915,00	2919,00	2194,30	2200,00
17000	283,33	127,25	127,10	3303,67	3304,00	2486,87	2494,00
19000	316,67	142,22	142,10	3692,33	3688,00	2779,45	2788,00
21000	350,00	157,19	157,50	4081,00	4086,00	3072,02	3081,00
23000	383,33	172,16	172,90	4469,67	4470,00	3364,59	3375,00
24000	400,00	179,64	180,20	4664,00	4650,00	3510,88	3521,00
25000	416,67	187,13	187,50	4858,33	4851,00	3657,17	3669,00
26000	433,33	194,61	194,50	5052,67	5049,00	3803,45	3815,00
27000	450,00	202,10	201,40	5247,00	5251,00	3949,74	3962,00
28000	466,67	209,58	209,20	5441,33	5448,00	4096,03	4019,00

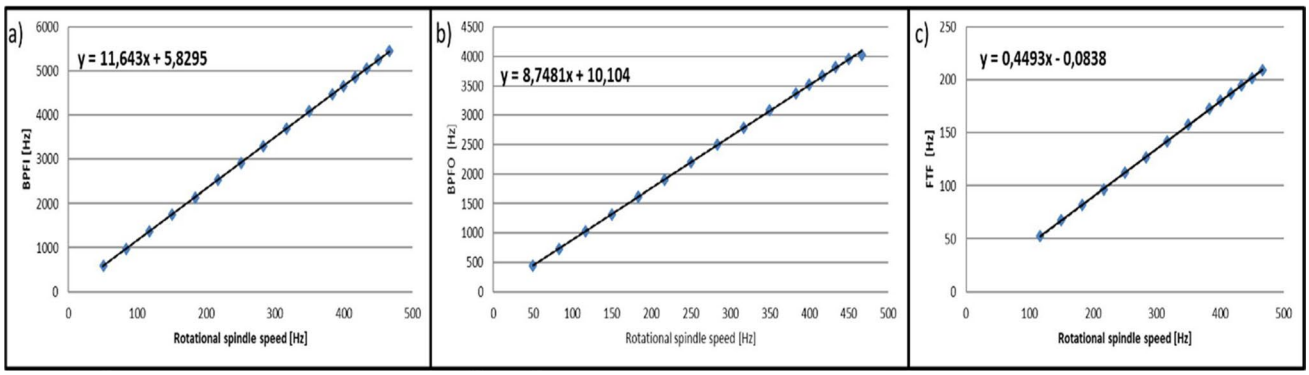

Fig. 4 **a** BPFO bearing fault frequencies as a function of spindle speeds. **b** BPFI bearing fault frequencies as a function of spindle speeds. **c** TFT bearing fault frequencies as a function of spindle speeds

The values of the defect frequencies extracted from the frequency spectra are plotted, as a function of the spindle speed for the frequencies BPFO (Fig. 4a), BPFI (Fig. 4b), and TFT (Fig. 4c). The curves confirm the linear relationship between the fault frequency and the spindle speed and the linearity factor presented by the slope of the line can be found. For Fig. 4a, the ratio between the BPFO fault frequency and the spindle speed is 11.64, 8.74 for the BPFI fault (Fig. 4b), and 0.44 for the TFT fault (Fig. 4c). these experimental values are close to the theoretical values provided by the manufacturer (Table 2).

Figure 5 shows a waterfall graph which is a view of successive FFT spectra taken at different spindle speeds. In other words. The *x*-axis represents the frequency, the *y*-axis is the spindle speed rotation and the *z*-axis is the amplitude. This waterfall graph is used to show the progression of frequencies' characteristics according to the spindle speed rotation. The evolution of the FTF as a function of the speed of rotation of the spindle can be observed and the appearance of the frequency of the electrical network at 60 Hz.

Another waterfall plot is the plot used to represent the signal in time–frequency such that the signal is decomposed to a several number of blocks with a constant time interval. The FFTs of these blocks are plotted in a cascade fashion. This representation is useful to track changes in the signal over a short period such as during machine run-up or coast-down.

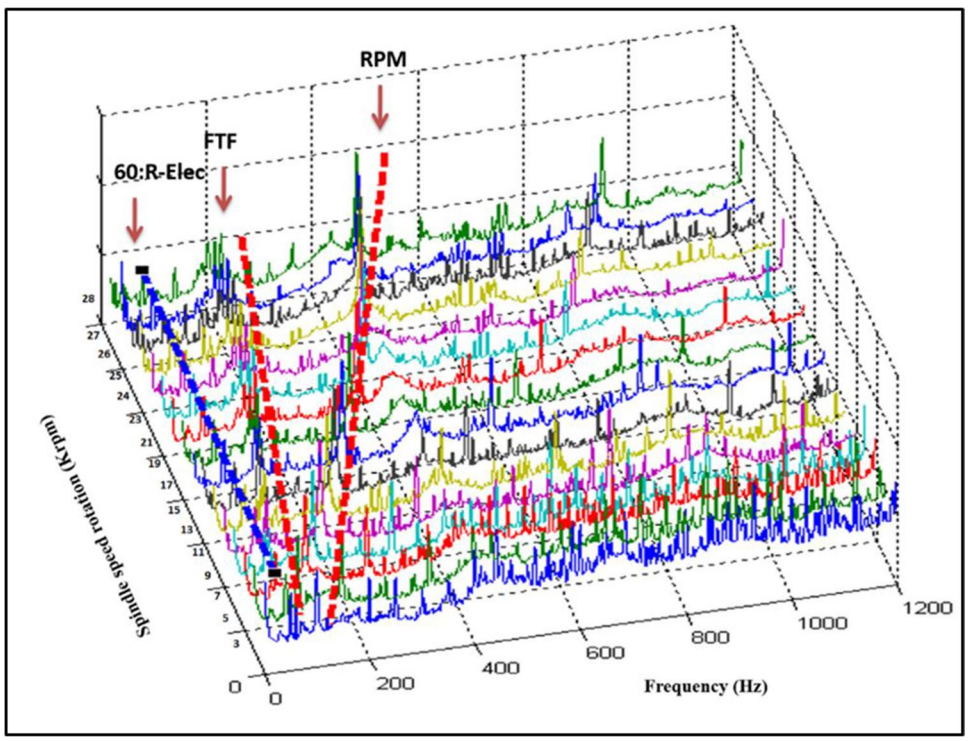

Fig. 5 Waterfall graph of accelerometers signals

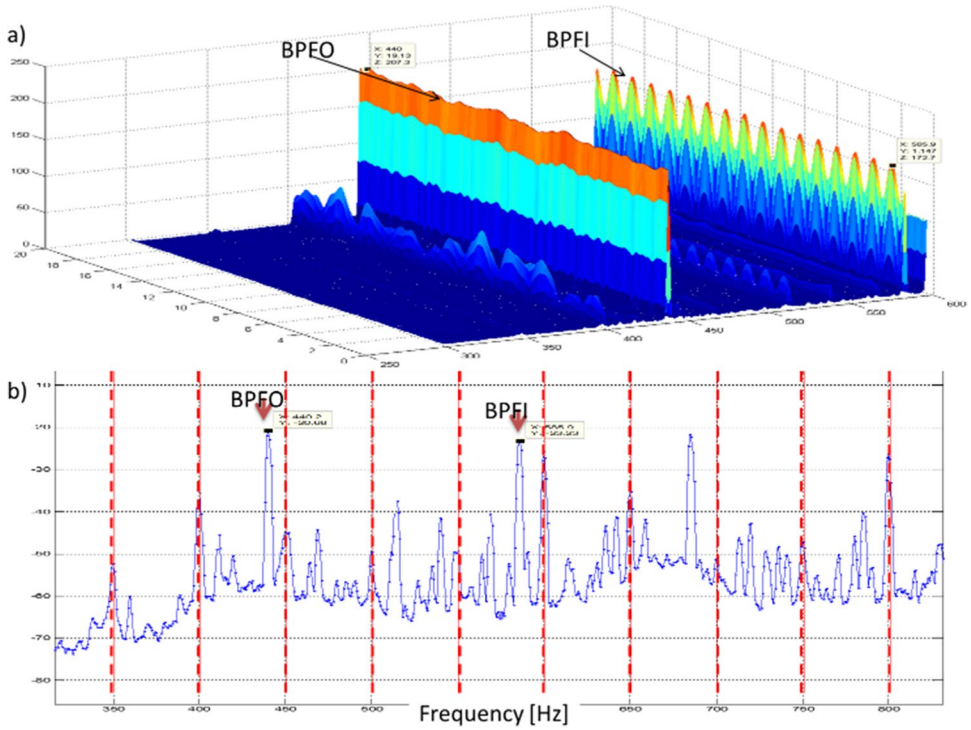

Fig. 6 **a** 3D time–frequency spectrogram of acceleration signal acquired at 3000 rpm in *Y* direction (250–600 Hz). **b** power spectra of the same signal estimated by welch algorithm. The dotted line in figure b shows the harmonics of the rotation speed

The frequency and amplitude of each component can be tracked and useful information such as resonance conditions can be found. In the next section, the signal is analyzed in time–frequency domain.

4.2 Time–frequency analysis

Non-stable regimes correspond to the operating states of a rotating machine with variations in its speed, mainly generated by start-up procedures, load change conditions, and operating disturbances. Under these conditions, usually caused by load and speed fluctuations, conventional signal processing techniques such as pure spectral analysis are ineffective in diagnosing machine faults [34]. To address this problem, time–frequency analysis offers the possibility of representing non-stationary signals in these two spaces. In this category, the short-time Fourier transform (STFT), the operation from which the spectrogram is determined,

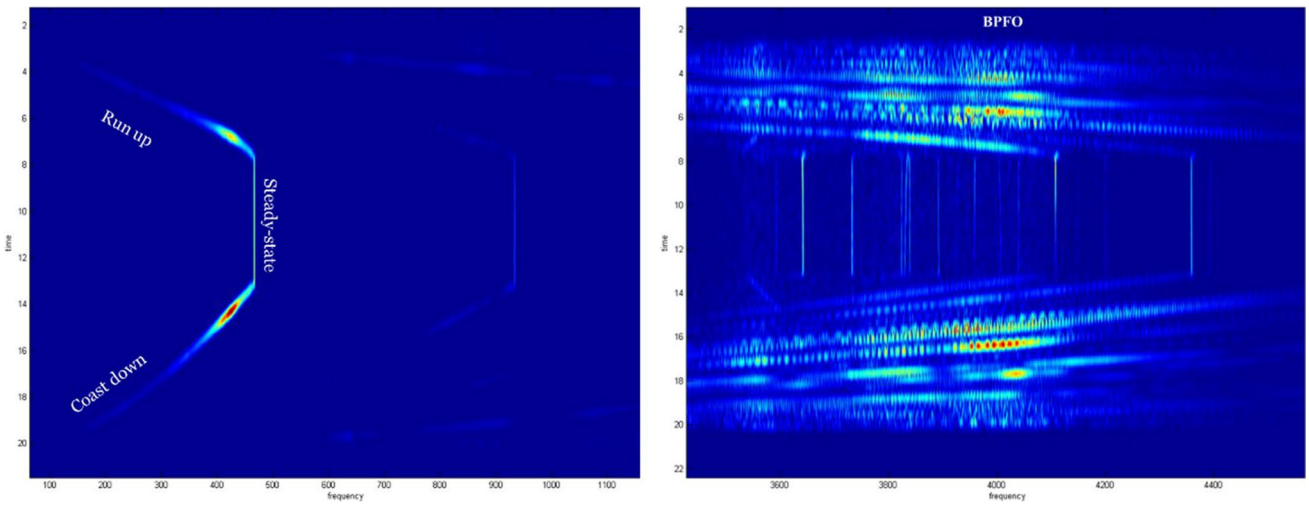

Fig. 7 Left) time–frequency spectrogram of acceleration signal acquired in run-up, steady-state and coast down in the frequency range of 0 at1100 Hz. Right) time–frequency spectrogram of acceleration signal acquired in run-up, steady-state, and coast-down in the frequency range of 3500 to 4600 Hz

has been widely applied for fault diagnosis in both stationary and non-stationary modes [35, 36]. The authors of [37] state that the major limitation of STFT analysis lies in the trade-off considered between the two dimensions in terms of resolution. A good localization in time requires the use of a small window, which therefore leads to a poor frequency resolution and vice versa.

Figure 6a and c shows the frequency-time spectrogram in 2D of vibration signal acquired at 3000 rpm in the frequency range of 250 at 600 Hz. The two frequency components of BFFO (440 Hz) and BPFI (585 Hz) frequencies can be seen.

If the operating conditions are not stationary, insofar as we consider a speed varying progressively from 0 to 466 Hz (28000 rpm) in run-up or coast-down, in transient conditions, and on a time–frequency spectrogram by fast Fourier transform (STFT) (Fig. 7). In Fig. 7 (Right), an amplification of vibration around the resonance frequencies of the bearing (4000 Hz) is observed; the excitation is coming from the shock generated at each ball passage on the defect, which excites the harmonics of BPFO.

4.3 Stationary statistics indicators

In the next set of graphs, four different vibration severity normalized indicators were evaluated for all spindles along their operating speed. These statistics are done for

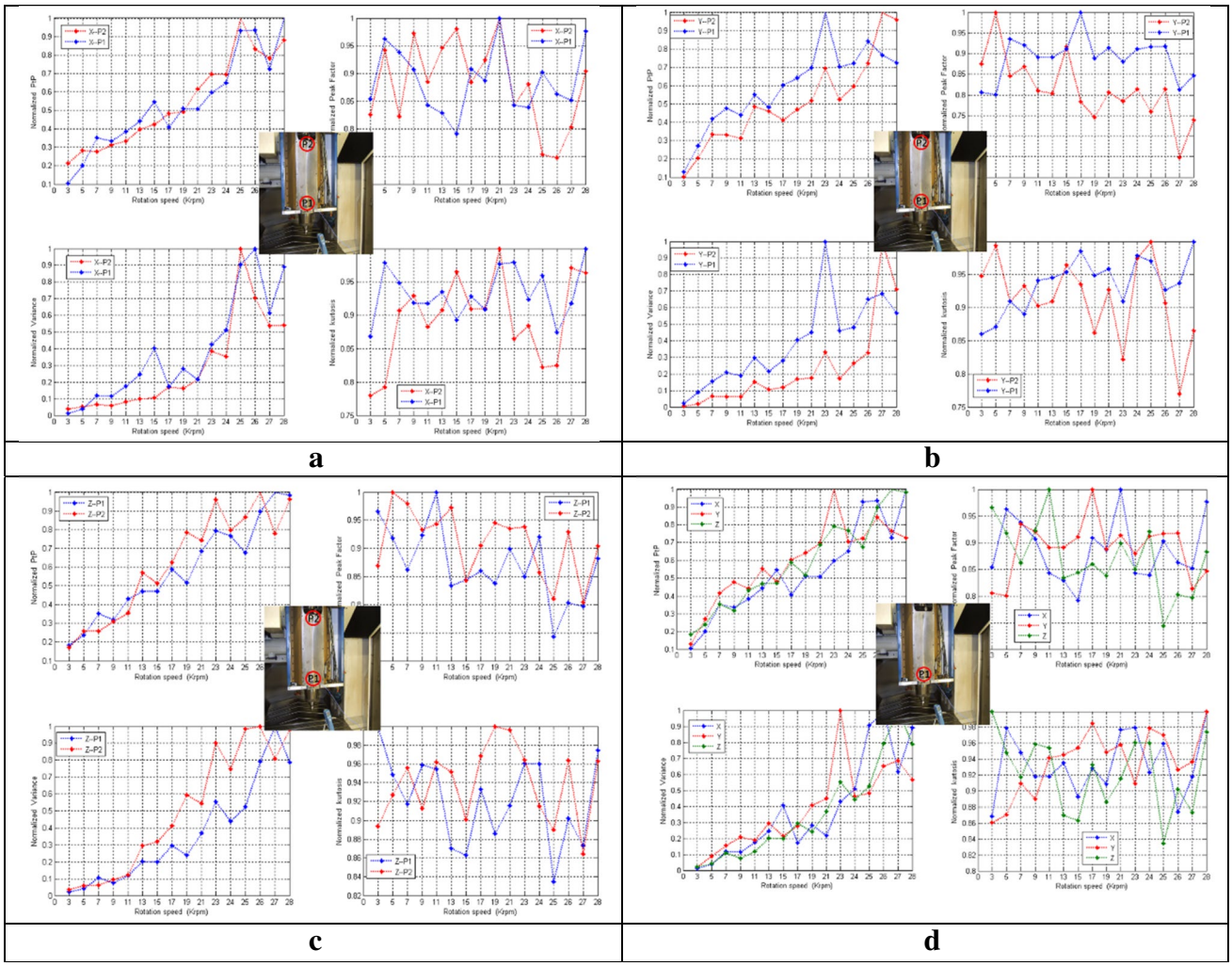

Fig. 8 **a** The evolution of normalized statistics (Peak to peak, crest factor, Variance, and kurtosis) as a function of the rotation spindle speed and the position of the accelerometer in *X* direction according to the two measurement points P1 and P2. **b** The evolution of normalized statistics (Peak to peak, crest factor, Variance, and kurtosis) as a function of the rotation spindle speed and the position of the accelerometer in *Y* direction according to the two measurement points P1 and P2. **c** The evolution of normalized statistics (Peak to peak, crest factor, Variance, and kurtosis) as a function of the rotation spindle speed and the position of the accelerometer in *Z* direction according to the two measurement points P1 and P2. **d** The evolution of normalized statistics (Peak to peak, crest factor, Variance, and kurtosis) as a function of the rotation spindle speed and the position of the accelerometer in *X*, *Y*, and *Z* directions according to the two measurement points P1

Table 5 Stationary statistics indicators

Crest factor	Peak-to-peak	Variance	Kurtosis
$\frac{\frac{1}{2}(\max(x_i)-\min(x_i))}{\sqrt{\frac{1}{N}\sum_{i=1}^{N}(x_i)^2}}$	$\max(x_i)-\min(x_i)$	$\frac{1}{N}\sum_{i=1}^{N}(x_i-\overline{x})^2$	$\frac{\frac{1}{N}\sum_{i=1}^{N}(x_i-\overline{x})^4}{(\frac{1}{N}\sum_{i=1}^{N}(x_i-\overline{x})^2)^2}$

both sensor positions as mentioned in paragraph 3.1 (see Fig. 1) and for *X*, *Y*, and *Z* directions. Figure 8a–c shows the evolution of normalized statistics as a function of the spindle speed rotation in the two positions of the accelerometer and according to the three directions *X*, *Y*, and *Z*. Figure 8d compares the results of one position (lower position of non-rotating part) and the different directions of acceleration (*X*, *Y*, and *Z*). These indicators are Crest factor, peak-to-peak, variance, and kurtosis, they are normalized to enclose their values from 0 to 1. The equation for calculating them is summarized as follows (Table 5).

Note that for the all spindles studied, each of the vibration severity indicators varies significantly along the spindle speed. The indicators peak-to-peak and variance trends to increase with speed in a similar manner, while variance increases slowly at low spindle speed than peak-to-peak indicator. Crest factor and kurtosis, on the contrary, tend to decrease in value with higher speed of the spindle when they are compared with their own initial values. Some peaks identify along spindle speed for these indicators, do not necessarily occur at critical speeds. These peaks are explained by high vibration amplitude at relatively low frequency (low energy). Because of the fluctuations of values among these severity indicators along the spindle speed, they must be used carefully when using them for evaluating spindle condition.

Most conventional vibration monitoring techniques assume that machines operate in a steady state and that the change in vibration behavior describes the evolution of the degradation state of the machine, thus neglecting the impact

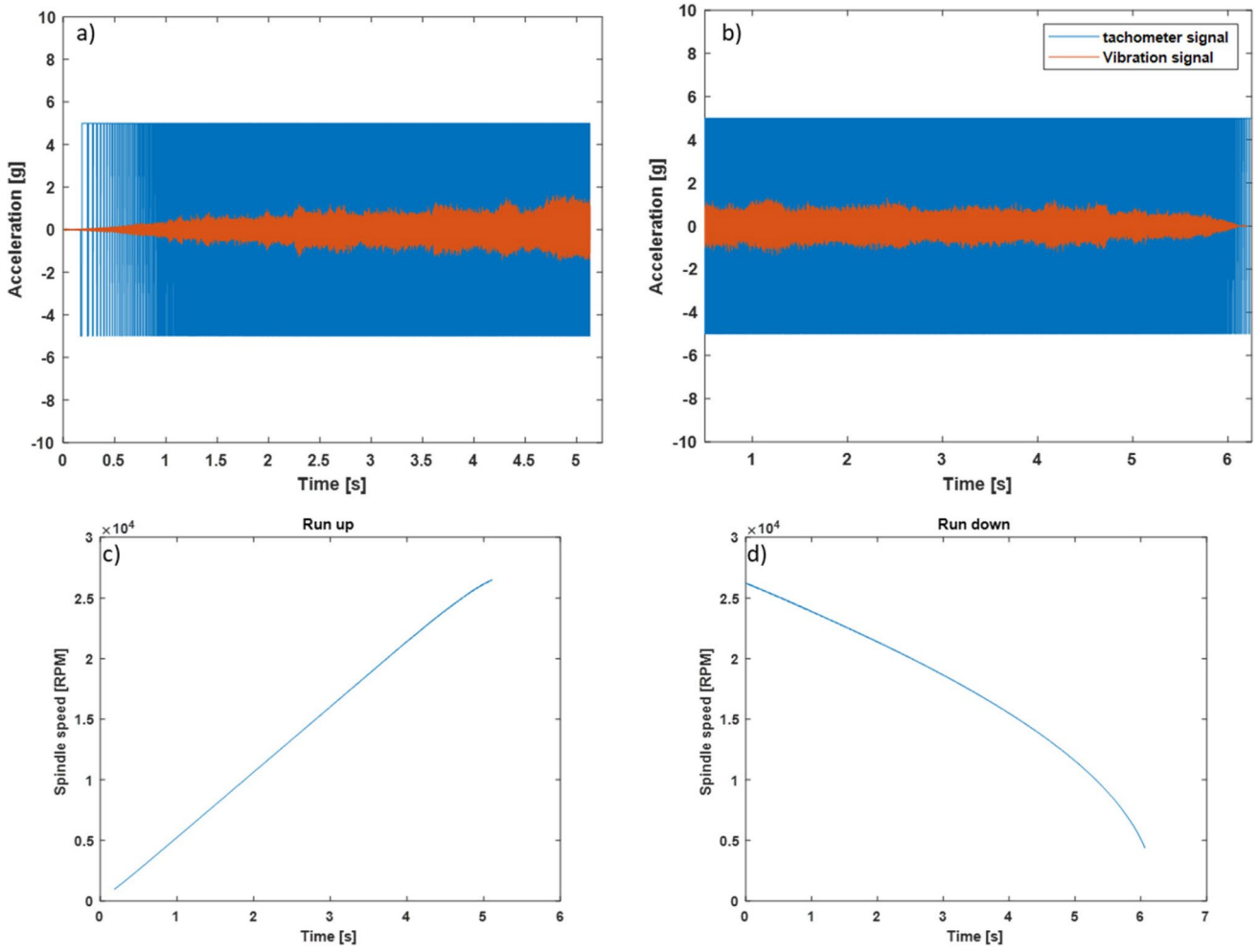

Fig. 9 **a** Run-up acceleration signal in red color and tachometer signal in blue color. **b** Coast-down acceleration signal in red color and tachometer signal in blue color. **c** RPM signal estimated from tachometer signal in run-up. **d** RPM signal estimated from tachometer signal in coast-down

caused by the variation of the operating conditions. However, the operation of machines operating in variable regimes practically rejects this hypothesis. Finding a method to compensate for the effects caused by the variation of the speed and the load is speed and load is, therefore, of significant practical value. Several approaches related to this problem have been limited to testing machines at no load or at conditions that do not often deviate from a steady state.

The following study shows how to analyze a vibration signal from a high-speed milling machine using order analysis. Order analysis is used to quantify noise or vibration in rotating machines whose rotational speed varies over time, in other words, under non-stationary conditions. An order refers to a frequency that is a certain multiple of a reference rotational speed. For example, a vibration signal with a frequency equal to twice the rotational frequency of a motor corresponds to an order of two, and similarly, a vibration signal with a frequency equal to 0.5 times the rotational frequency of the motor corresponds to an order of 0.5. In this paper, the high amplitude orders are determined to study the bearing fault from the high-speed milling vibration signals.

5 Order analysis

5.1 Introduction

In this study, vibration data from an accelerometer in a machine center's non-rotating spindle during the run-up and coast-down of the spindle motor are analyzed. In a center milling, the spindle, tool, and spindle bearings are just a few of the rotating parts. Each component rotates with respect to the main motor at a known, fixed rate, and each one could cause unwelcome vibration. The spindle motor's rotational speed as well as frequency faults in the spindle bearings can both affect the frequency of the dominant vibration components. Important center milling-related vibrational components can be detected at integer multiples of the spindle's rotational frequency and at non-integer multiples of the bearing frequencies.

The signal in this study is a time-dependent acceleration in g (Fig. 9a, b), sampled at a rate *Fs* equal to 48000 Hz. The data used include RPM, the angular speed of the according to the time instants. A spindle speed signal commonly consists of a sequence of tachometer pulses (Fig. 9a, b). The pulse sites of a bilevel tachometer waveform are identified, extract the RPM signal from the tachometer pulse signal, and compute the pulse interval to determine rotational speed. The predicted RPM signals are shown in Fig. 9c, d in the run-up and coast-down conditions, respectively. Figure 9 shows spindle speed, in run-up and coast-down operations, and vibration signal acquired. The spindle of the machining center rotates from 0 to 28000 rpm in run-up regime or from 28000 to 0 rpm in coast-down regime and the spindle speed increases during the run-up and decreases in the coast-down. Therefore, the vibration amplitude changes as a function of rotational speed. This type of RPM profile is typical for analyzing vibration in rotating machinery, among others high-speed machining.

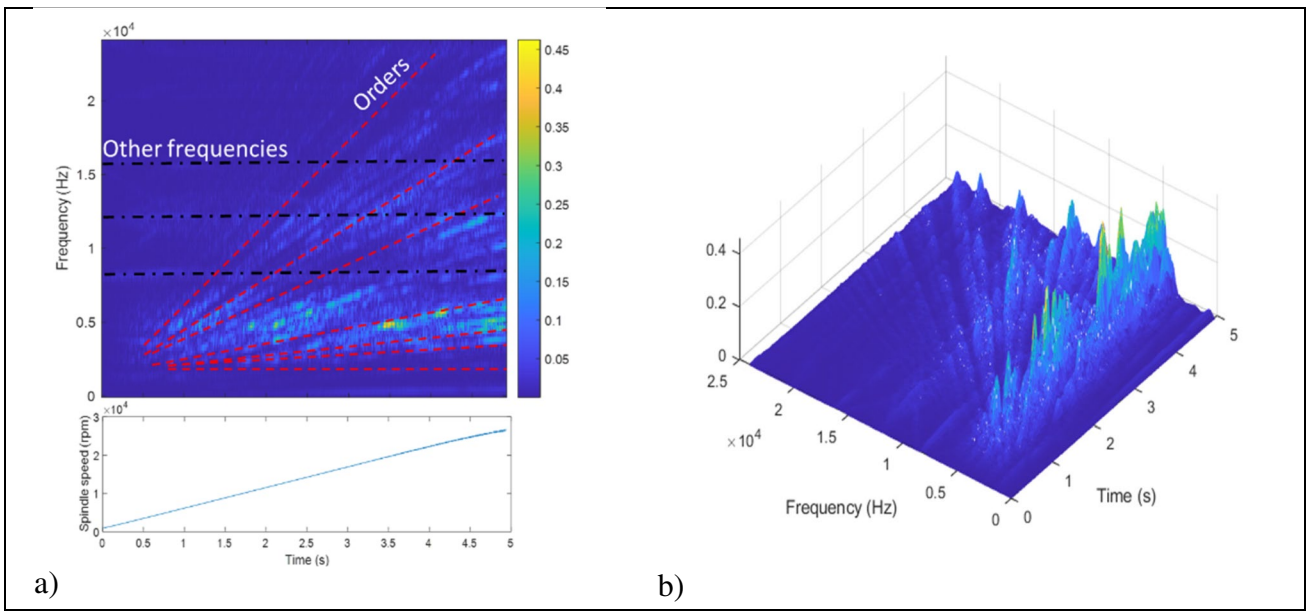

Fig. 10 **a** RPM-frequency map for the vibration data in run-up case, diagonal dashed lines present orders, and horizontal lines present other frequencies. **b** 3D RPM-frequency map for the vibration data in run-up case

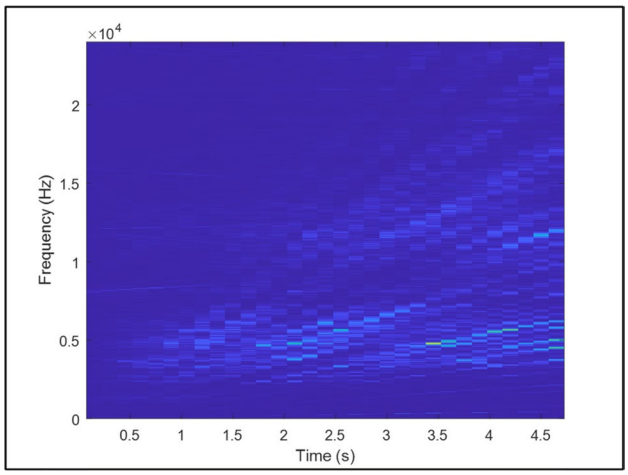

Fig. 11 **a** RPM-frequency map for the vibration data in run-up case, the frequency resolution is 5 Hz

5.2 RPM-frequency map vs RPM-order map

The short-time Fourier transform of the vibration signal yields an RPM-frequency map, which can be used to visualize the vibration signal in the frequency domain.

An RPM-frequency map, an RPM versus time curve, and several numerical indicators that can be used to quantify vibration components are all included in Fig. 10. Root-mean-square (RMS) amplitude is represented by the map's amplitude. The waterfall plot generates a three-dimensional is generated and is shown in Fig. 10b.

Many of the tracks have frequencies that change with spindle speed in the RPM frequency maps (here, the acceleration regime is shown). The tracks may be orders of the spindle's rotational frequency, according to this evidence. Near the RPM peak, there are components with high amplitude and frequencies between 4 and 6 kHz. The resolution is equal to 30 Hz. A Hann window is used. Some frequency components might be more easily resolved if the resolution were set to a lower value. For instance, at peak RPM, the low-frequency components are not separated. The high amplitude tracks seem to mix at low RPM values.

The RPM-frequency map to resolve these components is shown in Fig. 11 with a resolution of 5 Hz. At the peak RPM, the low-frequency components can now be distinguished, but as the RPM changes more quickly, there is significant smearing. As the motor speed increases or decreases, the vibration orders change the frequency in each time window, resulting in a wider spectral track. Due to the longer time windows needed for finer resolution, this smearing effect is more pronounced. In this instance, the increase in smearing artifacts during the acceleration and deceleration phases was brought on by the improvement in spectral resolution. This compromise can be avoided by creating an order map.

For the order analysis, Fig. 12 shows a spectral map of order versus RPM. By resampling the signal at fixed phase increments and creating a stationary sinusoid for each order, the technique eliminates smearing artifacts. In order to process the resampled signal, a quick Fourier transform is used. Since the reference spindle rotation speed is a fixed multiple of each order. The spectral axis of the map is now order

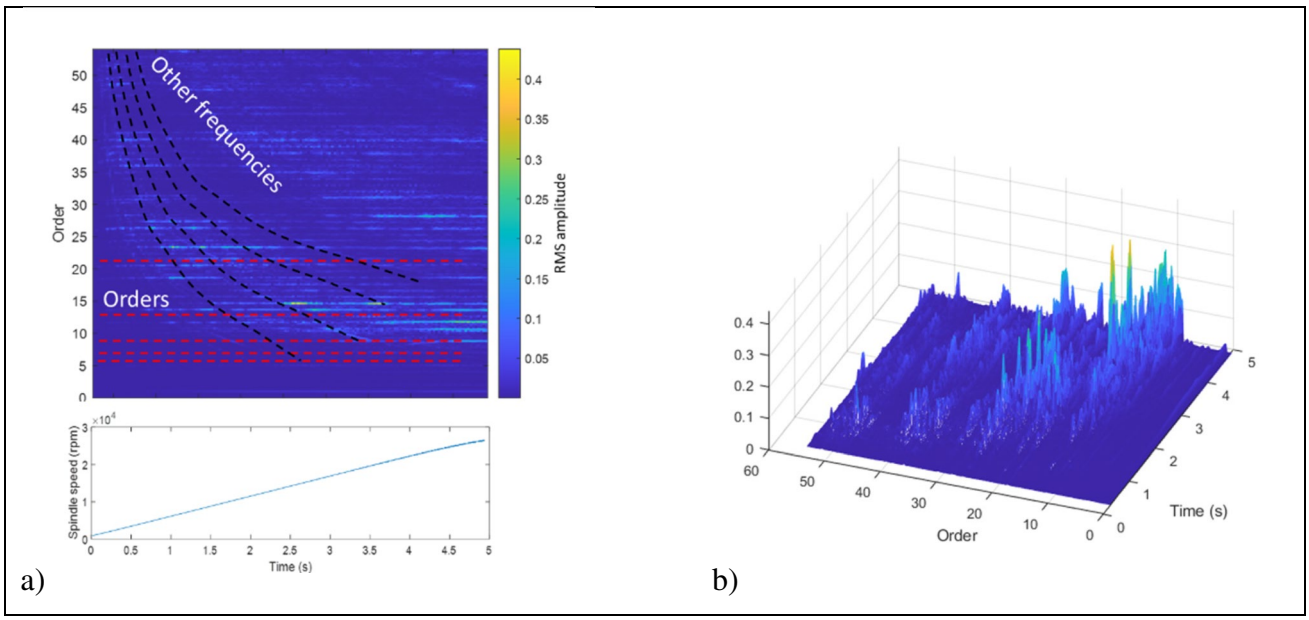

Fig. 12 **a** RPM-Order map for the vibration data in run-up case, horizontal dashed lines present orders, and curved lines present other frequencies. **b** 3D RPM-Order map for the vibration data in run-up case. The order resolution is 0.005

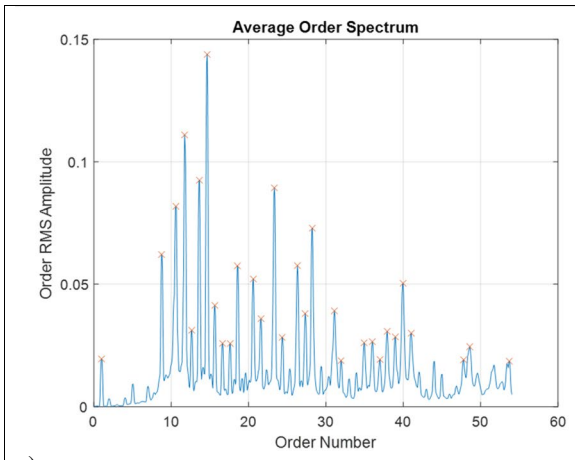

a)

Peak	Order Value	Peak	Order Value
1	14.6520	16	12.6630
2	11.7350	17	37.9230
3	13.6570	18	41.0390
4	23.3370	19	38.9830
5	10.6080	20	24.3310
6	28.2430	21	36.0000
7	8.7510	22	34.9390
8	26.3200	23	16.6410
9	18.5640	24	17.6350
10	20.6190	25	48.5970
11	39.9780	26	0.9940
12	15.6460	27	36.9940
13	31.0940	28	47.8010
14	27.3150	29	31.9560
15	21.6130	30	53.7020

b)

Fig. 13 **a** Average order spectrum. Order RMS amplitude according to the order number. **b** Order value extracted from average order spectrum

rather than frequency, and the resolution parameter is now expressed in orders rather than Hz. This map is computed in a flat-top window. 0.06 is the resolution's value.

Each order's straight-line trace on the map demonstrates that the vibration occurs at a constant multiple of the spindle speed. It is simple to connect each spectral component to the spindle speed using the order maps. Comparing this to the RPM frequency map, smearing artifacts are significantly reduced.

5.3 Average order spectrum

The RPM-Order map is used to evaluate the average order spectrum by computing the RMS amplitude for each order and determine the locations of the peaks of the order map. Figure 13a shows the average order spectrum which is a presentation of the RMS amplitude according to the order number. Order values corresponding to 30 peaks are extracted (see Fig. 13b). The peaks of the spectrum correspond to the ridges seen in the order-RPM map (Fig. 13).

Order values which are integer multiples represent the order of the spindle rotation ($k.O1$), where vibration generated by this spindle would occur. $O1$ represents the spindle rotation order and k in an integer. On the other hand, order values which are not integer multiples correspond to the bearing order faults, their harmonics, and the lateral bands of amplitude modulation by the rotation of the spindle, more specifically to the $BPOI$, $BPOO$,.$BPPI$, $k.BPOO$, $k.BPOI \pm n.O1$, and $k.BPOO \pm n.O1$.

$BPOO$ is the ball pass order outer, $BPOI$ is the ball pass order inner, $O1$ is the spindle rotation order, and k are integers.

Table 6 Orders values of spindle rotation and bearing faults

Peak	Order Value	Characteristic	Peak	Order Value	Characteristic
1	14.6520	OBPFI+3.O1	16	12.6630	OBPFI+1
2	11.7350	OBPFI	17	37.9230	3*OBPFI+3
3	13.6570	OBPFI+2.O1	18	41.0390	41*O1
4	23.3370	2*OBPFI	19	38.9830	39.O1
5	10.6080	OBPFI-1.O1	20	24.3310	2*OBPFI+1
6	28.2430	3*OBPFO+2	21	36.0000	36.O
7	8.7510	OBPFO	22	34.9390	3*OBPFI
8	26.3200	3*OBPFO	23	16.6410	2*OBPFI-1
9	18.5640	2*BPFO+1	24	17.6350	2*OBPFO
10	20.6190	2*BPFO+3	25	48.5970	4*OBPFI+2
11	39.9780	40.O1	26	0.9940	O1
12	15.6460	2*OBPFO-2	27	36.9940	37.O1
13	31.0940	31*O1	28	47.8010	4*OBPFI
14	27.3150	3*OBPFO+1	29	31.9560	3*OBPFI-3
15	21.6130	2*OBPFI-2	30	53.7020	

O1	1
OBPFO	8,77
OBPFI	11,66

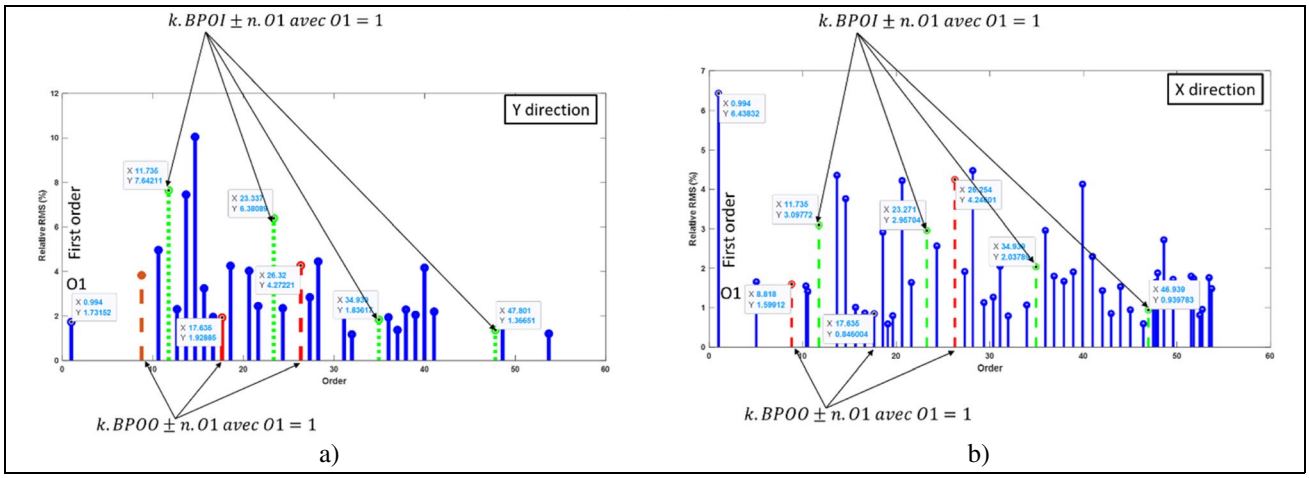

Fig. 14 Relative RMS according to the order for vibration signal in run-up regime and in X (**b**) and Y (**a**) direction. Green dotted lines present BPOI order, its harmonics, and its bands modulation. Red dashed lines present BPOO its harmonics and its bands modulation

The presence of lateral bands modulating the orders of the bearing defect confirms the bearing defect and its severity depends on the number of components in this band. Note that the maximum value of the order does not exceed the value of $\{\frac{fs}{2 \times \max\left(\frac{\text{RPM}}{60}\right)}\}$.

5.4 Relative RMS vs order

Table 6 is used to plot the relative RMS graph as a function of the order. The spindle rotation order and its harmonics, the BPOO and BPOI fault orders, their harmonics, and their modulations by spindle rotation can be identified. Figure 14 shows the graphs for the X and Y directions; the same observations are noted. This type of graph seems relevant for monitoring bearing defects in non-stationary conditions, in particular for high-speed machining centers, despite the stresses that the spindle will be able to withstand at high speeds and the non-linearities that may appear, among other the gyroscopic effect.

In [27], a study was conducted on the relationship between envelope analysis and spectral correlation in the

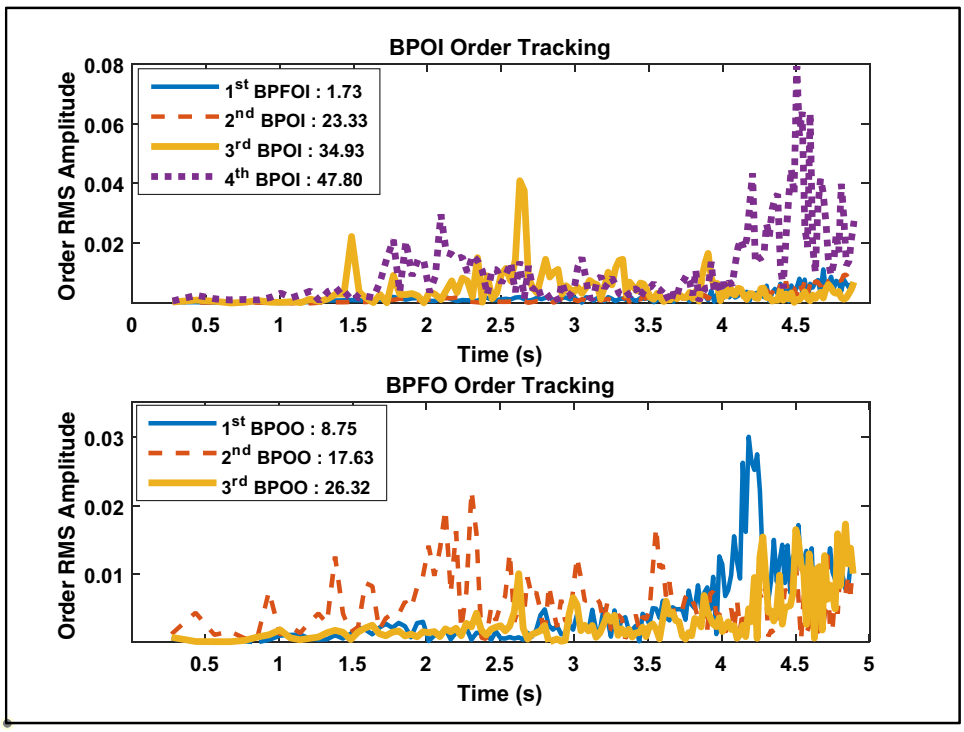

Fig. 15 RMS amplitude of BPOI and BPOO order tracking over time

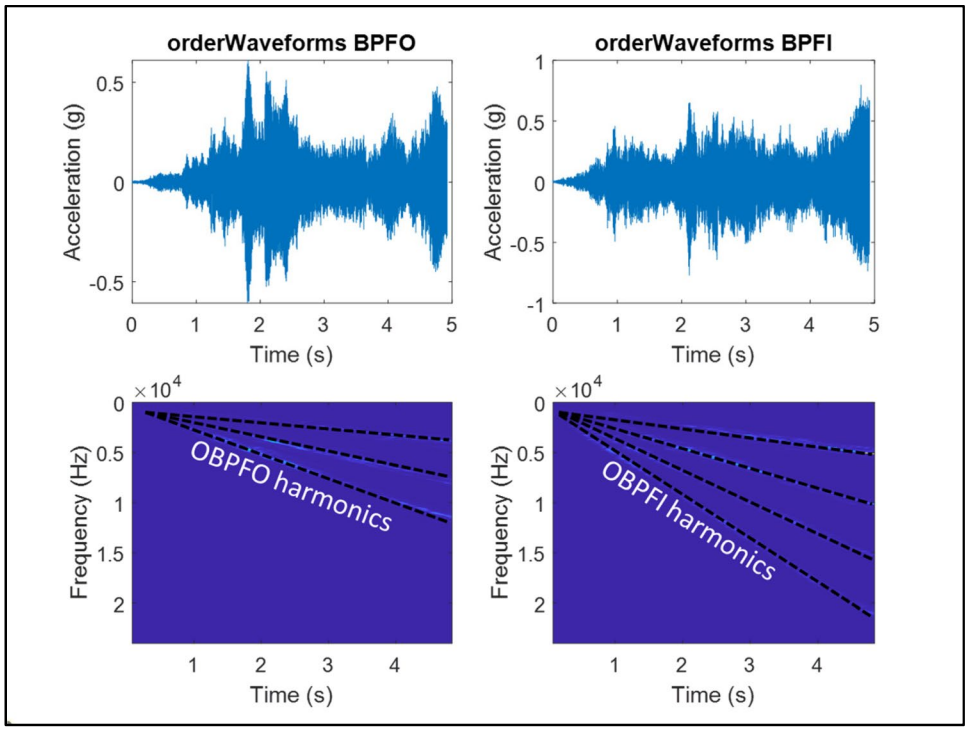

Fig. 16 Order waveforms BPOO and BPOI

diagnosis of bearings operating at variable speeds. It has been verified that the variation of the load causes a modulation at the level of the amplitude of impulsive events and thus increases the slippage effect which manifests itself at the level of the spectrum. In addition, varying the rotational speed spreads the characteristic spectrum of the faulty bearing by adding a frequency modulation component to the already amplitude-modulated signal.

Figure 15 shows the evolution over time of the RMS amplitude of the BPOI and BPOO orders and the first three harmonics. The sudden increase in RMS at certain times is noted, this is perhaps due to the crossing with the resonances of the bearings. Harmonics orders increase in amplitude slowly as the rotational speed of the spindle increases.

Next, a time-domain order waveform is extracted for each peak order using Vold-Kalman filter. Order waveforms can be compared directly to the original vibration and can be used also to monitor bearing faults. Figure 16 shows the order waveforms of BPOO, BPFI, and their harmonics in time and time–frequency domains.

Figure 17 shows a 3D waterfall, the contribution of each order in the frequency domain. On the energetic level, the

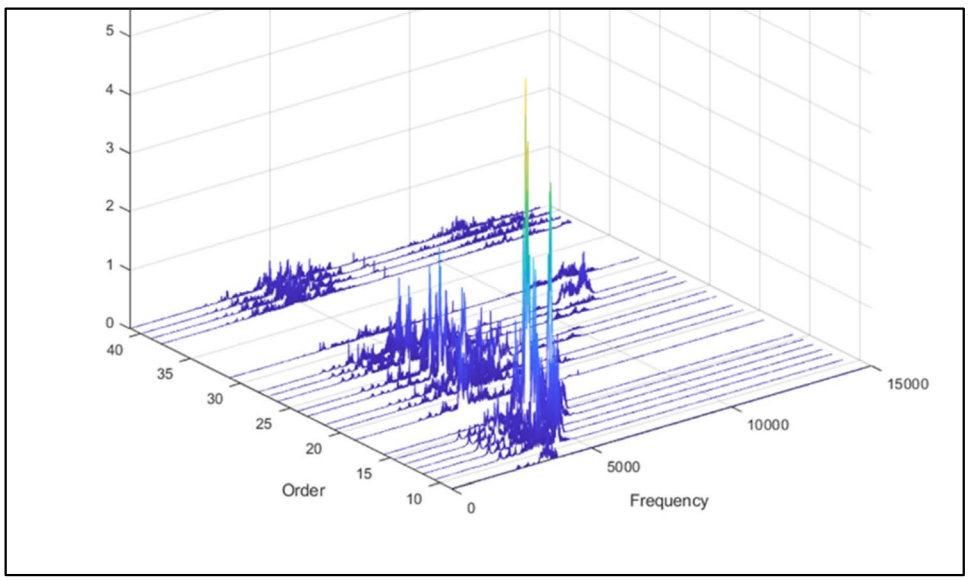

Fig. 17 3D waterfall diagram, frequency representation for each order component

presence of three classes can be observed. The first 15 orders contribute the most, then from order 20 to order 30 participates moderately.

6 Conclusion

In order to identify wear and flaws in moving parts and fix them before the machine breaks down, vibration analysis of rotary milling machines is a crucial component of industrial predictive maintenance programs. This leads to lower operating and maintenance expenses. In order to identify bearing defects in high-speed milling centers, this research suggests a vibration analysis technique based on tachometer order monitoring. This technique has never been used on high-speed machining centers to find spindle bearing flaws, but it is effective for rotating machine status monitoring in non-stationary processes. Tachometer order tracking is a frequency analysis method that uses multiple operating speeds (orders), instead of absolute frequencies (Hz), as the frequency base. Order tracking data acquisition uses information issued from the tachometer to sample at a rate proportional to spindle speed. A calculated order tracking process samples at a constant rate (i.e., Δt uniform), and then uses an algorithm to resample the data at constant angular increments. Different signal processing tools are proposed to detect bearing faults in high spindle milling centers in stationary and non-stationary conditions. Firstly, RPM-order map is computed, analyzed, and compared with RPM-frequency map. This tool seems the most relevant to analyze milling signals in non-stationary conditions and at high spindle speeds. Furthermore, Average order frequency is used to highlight the presence of bearing faults and the correspondence between fault frequencies and fault orders. At the end, Relative RMS order presentation is extracted, this diagram is useful and presents the severity of faults through the modulation component of bearing faults. In this paper, signals are analyzed by classical tools in stationary conditions to show their limits under the non-stationary conditions. An important interest must be taken in the bandwidth of the accelerometer. in fact, the characteristic frequencies of defects appear in the high frequencies, especially when the speed of the spindle reaches 28,000 rpm. The sampling frequency must be taken as the highest value to maximize the range of the commands.

Acknowledgements The author would like to thank the Ecole de Technologie Supérieure's Products, Processes, and Systems Engineering Laboratory in Montréal and Marc Thomas for their technical collaboration.

Author contribution The author has totally contributed to realizing this work, starting from the state of the art, the experimental part until the development and analysis of the results.

Funding Funding for this project was offered by the research laboratory LASPI of Jean Monnet University in France. The author would like to thank the Ecole de Technologie Supérieure in Montréal (Canada) and Professor Marc Thomas for their technical collaboration in the products, processes, and systems engineering Laboratory.

Data availability The authors also declare that they have full control of all primary data and that they agree to allow the journal to review their data if requested.

Declarations

Competing interests The authors declare no competing interests.

References

1. Schmidt S, Heyns PS, de Villiers JP (2018) A novelty detection diagnostic methodology for gearboxes operating under fluctuating operating conditions using probabilistic techniques. Mech Syst Signal Process 100:152–166. https://doi.org/10.1016/j.ymssp.2017.07.032
2. Ruiz-Cárcel C, Jaramillo VH, Mba D, Ottewill JR, Cao Y (2016) Combination of process and vibration data for improved condition monitoring of industrial systems working under variable operating conditions. Mech Syst Signal Process 66–67:699–714. https://doi.org/10.1016/j.ymssp.2015.05.018
3. Peeters C, Antoni J, Leclère Q, Verstraeten T, Helsen J (2022) Multi-harmonic phase demodulation method for instantaneous angular speed estimation using harmonic weighting. Mech Syst Signal Process 167. https://doi.org/10.1016/j.ymssp.2021.108533
4. Stander C, Heyns P, Schoombie W (2002) Using vibration monitoring for local fault detection on gears operating under fluctuating load conditions. Mech Syst Signal Process 16:1005–1024. https://doi.org/10.1006/mssp.2002.1479
5. Antoni J (2007) Cyclic spectral analysis in practice. Mech Syst Signal Process 21:597–630. https://doi.org/10.1016/j.ymssp.2006.08.007
6. Urbanek J, Barszcz T, Antoni J (2013) Time–frequency approach to extraction of selected second-order cyclostationary vibration components for varying operational conditions. Measurement 46:1454–1463. https://doi.org/10.1016/j.measurement.2012.11.042
7. Salameh JP, Cauet S, Etien E, Sakout A, Rambault L (2018) Gearbox condition monitoring in wind turbines: a review. Mech Syst Signal Process 111:251–264. https://doi.org/10.1016/j.ymssp.2018.03.052
8. Zhang L, Lang ZQ (2018) Wavelet energy transmissibility function and its application to wind turbine bearing condition monitoring. IEEE Trans Sust Energy 9:1833–1843. https://doi.org/10.1109/TSTE.2018.2816738
9. Wang F, Garcia-Sanz M (2018) Wind farm cooperative control for optimal power generation. Wind Engineering 0309524X18780377. https://doi.org/10.1177/0309524X18780377
10. Astolfi D (2019) A study of the impact of pitch misalignment on wind turbine performance. Machines 7:8. https://doi.org/10.3390/machines7010008
11. Ouanas A, Medoued A, Mordjaoui M, Lebaroud A, Sayad D (2018) Fault diagnosis in yaw drive induction motor for wind

turbine. Wind Eng 42:576–595. https://doi.org/10.1177/0309524X18780379
12. Yang C, Qian Z, Pei Y, Wei L (2018) A data-driven approach for condition monitoring of wind turbine pitch systems. Energies 11:2142. https://doi.org/10.3390/en11082142
13. Castellani F, Astolfi D, Becchetti M, Berno F, Cianetti F, Cetrini A (2018) Experimental and numerical vibrational analysis of a horizontal-axis micro-wind turbine. Energies 11:456. https://doi.org/10.3390/en11020456
14. Hendén J (2015) Book Servicing spindles at SKF (Autumn 2015)
15. Abele E, Korff D (2011) Avoidance of collision-caused spindle damages—challenges, methods and solutions for high dynamic machine tools CIRP Ann Manuf Technol 60:225–228. https://doi.org/10.1016/j.cirp.2011.03.031
16. De Castelbajac C (n.d.) Advance monitoring and improvement of HSM process. (In French). Original title: surveillance avancée et amélioration du procédé d'UGV. PhD thesis of the University of Nantes
17. De Castelbajac C, Ritou M, Laporte S, Furet B (2014) Monitoring of distributed defects on HSM spindle bearings. Appl Acoust 77:159–168. https://doi.org/10.1016/j.apacoust.2013.07.008
18. Wang C, Cheng K, Rakowski R, Soulard J (2018) An experimental investigation on ultra-precision instrumented smart aerostatic bearing spindle applied to high-speed micro-drilling. J Manuf Process 324–335. https://doi.org/10.1016/j.jmapro.2017.11.022
19. Yang H, Li G, He J et al (2022) Health condition evaluation method for motorized spindle on the basis of optimised VMD and GMM-HMM. Int J Adv Manuf Technol. https://doi.org/10.1007/s00170-022-10202-6
20. Cao H, Zhang X, Chen X (2017) The concept and progress of intelligent spindles: a review. Int J Mach Tools Manuf 112:21–52. https://doi.org/10.1016/j.ijmachtools.2016.10.005 (ISSN 0890-6955)
21. Hoshi T (2006) Damage monitoring of ball bearing. CIRP Ann 55(1):427–430. https://doi.org/10.1016/S0007-8506(07)60451-X
22. Neugebauer R, Fischer J, Praedicow M (2010) Condition-based preventive maintenance of main spindles. Prod Eng Res Dev. https://doi.org/10.1007/s11740-010-0272-z
23. Abboud D (2016) Vibration-based condition monitoring of rotating machines in nonstationary regime, Phd Thesis INSA de Lyon. HAL Id : tel-01370989, version 1
24. Chen K, Zhang X, Zhao Z et al (2021) Milling chatter monitoring under variable cutting conditions based on time series features. Int J Adv Manuf Technol 113:2595–2613. https://doi.org/10.1007/s00170-021-06746-8
25. Zhao D, Li J, Cheng W, He Z (2019) Generalized demodulation transform for bearing fault diagnosis under nonstationary conditions and gear noise interferences. Chin J Mech Eng 32(1). https://doi.org/10.1186/s10033-019-0322-1
26. Abboud D, Antoni J (2016) Order-frequency analysis of machine signals. Mech Syst Signal Process 0–1. https://doi.org/10.1016/j.ymssp.2016.10.024
27. Borghesani P, Pennacchi P, Randall RB, Ricci R (2012) Order tracking for discrete-random separation invariable speed conditions. Mech Syst Signal Process 30:1–22. https://doi.org/10.1016/j.ymssp.2012.01.015
28. Borghesani P, Ricci R, Chatterton S, Pennacchi P (2013) A new procedure for using envelope analysis for rolling element bearing diagnostics in variable operating conditions. Mech Syst Signal Process 38:23–35. https://doi.org/10.1016/j.ymssp.2012.09.014
29. Zhao M, Lin J, Xu X, Lei Y (2013) Tacholess envelope order analysis and its application to fault detection of rolling element bearings with varying speeds. Sensors 1310856–10875. https://doi.org/10.3390/s130810856
30. Brandt A (2011) Book noise and vibration analysis: signal analysis and experimental procedures. John Wiley & Sons, Chichester
31. Yue A, Gao H, Liu X, Liang SY, Wang L (2019) A review of chatter vibration research in milling. Chin J Aeronaut 32(2):215–242. https://doi.org/10.1016/j.cja.2018.11.007
32. Forestier F, Gagnol V, Ray P, Paris H (2011) Modeling of self-vibratory drilling head-spindle system for predictions of bearings lifespan. Adv Acoust Vib 2011:606087. https://doi.org/10.1155/2011/606087
33. Heitz T, He N, Chen N et al (2022) A review on dynamics in micro-milling. Int J Adv Manuf Technol 122:3467–3491. https://doi.org/10.1007/s00170-022-10014-8
34. Vicuñan CM, Chaari F (2016) Analysis of a planetary gearbox under non-stationary operating conditions: chapter: numerical and experimental results, in: published in: advances in condition monitoring of machinery in non-stationary operations publisher: Springer International Publishing. https://doi.org/10.1007/978-3-319-20463-5_26
35. Chaari F, Zimroz R, Bartelmus W, Haddar M (Eds.) (2016) Advances in condition monitoring of machinery in non-stationary operations, 4th int. conf. on condition monitoring of machinery in non-stationary operations 2014, Lyon, France, 15 December 2014, in: Applied Condition Monitoring, Springer, Cham, Switzerland, pp.351–362. ISBN: 978–3–642–39348–8
36. Zimroz R, Bartelmus W (2009) Gearbox condition estimation using cyclo-stationary properties of vibration signal. Key Eng Mater 413:471–478. https://doi.org/10.4028/www.scientific.net/KEM.413-414.471
37. Chaari R, Khabou MT, Barkallah M, Chaari F, Haddar M (2016) Dynamic analysis of gearbox behaviour in milling process: non-stationary operations. Proc Inst Mech Eng C J Mech 19:3372–3388. https://doi.org/10.1177/0954406215590170